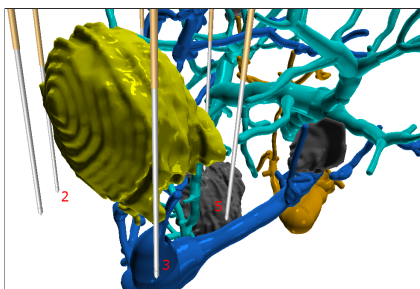


Visually Supporting Multiple Needle Placement in Irreversible Electroporation Interventions

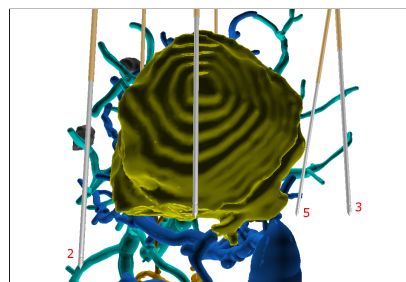
J. Kreiser¹ and J. Freedman² and T. Ropinski¹

¹Visual Computing Group, Ulm University, Germany

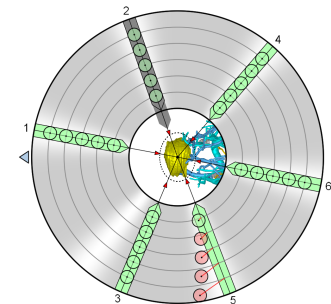
²Karolinska Institutet Stockholm, Sweden



(a) Conventional visualization communicating needle placement in 3D.



(b) A change in perspective reveals the misplacement of several needles. Needle 2 is too deep, 3 too far away, and 5 not parallel.



(c) The proposed radial visualization clearly communicates needle misplacement without the adaptation of viewing parameters.

Figure 1: Needle placement in irreversible electroporation (IRE) requires certain parameters (position, parallelism, depth) to be met. The task of fulfilling these requirements is complex and time-consuming. In conventional visualizations, occlusions can hinder the procedure (a), (b). In contrast, our visualization communicates all necessary parameters and allows for an optimal needle placement (c).

Abstract

Irreversible electroporation (IRE) is a minimally invasive technique for small tumor ablation. Multiple needles are inserted around the planned treatment zone and, depending on the size, inside as well. An applied electric field triggers instant cell death around this zone. To ensure the correct application of IRE, certain criteria need to be fulfilled. The needles' placement in the tissue has to be parallel, at the same depth, and in a pattern which allows the electric field to effectively destroy the targeted lesions. As multiple needles need to synchronously fulfill these criteria, it is challenging for the surgeon to perform a successful IRE. Therefore, we propose a visualization which exploits intuitive visual coding to support the surgeon when conducting IREs. We consider two scenarios: first, to monitor IRE parameters while inserting needles during laparoscopic surgery; second, to validate IRE parameters in post-placement scenarios using computed tomography (CT). With the help of an easy to comprehend and lightweight visualization, surgeons are enabled to quickly visually detect what needs to be adjusted. We have evaluated our visualization together with surgeons to investigate the practical use for IRE liver ablations. A quantitative study shows the effectiveness compared to a single 3D view placement method.

Categories and Subject Descriptors (according to ACM CCS): I.3.3 [Computer Graphics]: Picture/Image Generation—Display algorithms

1. Introduction

In current surgeries, tumor ablations are a common type of therapy. While modern ablations are suitable to treat larger lesions, they come with the downside that healthy regions are also damaged. Therefore, the goal is to further reduce the degree of invasiveness, which results in less stress on the patient's body and thus supports faster recovery. A wide range of such minimally invasive surgery techniques exist, many of which rely on imaging methods like computed tomography (CT),

ultrasound (US) imaging, or are performed laparoscopically with the support of a monoscopic or a stereoscopic camera [Mac01].

Irreversible Electroporation (IRE) is a surgical intervention, during which multiple needles are positioned around small tumors. Optionally central probes can be introduced for larger targets, and a high-voltage (~1.5-3kV) is applied in short pulses [Nar11]. The resulting electric field causes holes in the tumor cells' membranes, which is an irreversible process that triggers cell death. The advantages of this intervention compared to others, e.g. radiofrequency thermal

ablation (RFA) or cryotherapy, are fewer collateral injuries [MILR07] and a more area independent treatment. Thus, ablations can be performed closer to major vessels and nerves, which enables ablations of lesions previously not accessible. Furthermore, while thermal ablations often have problems with the *heat/cold sink effect* [LTK10], meaning that major blood vessels cool down or reheat treated areas during the ablation process, IRE is unaffected by the blood flow and hence is not impaired by these side effects. Due to these benefits, recently IRE techniques are becoming more and more popular for treating lesions, in the pancreas, the prostate, the kidneys and the liver.

However, to support a successful IRE treatment some requirements must be fulfilled. The parallelism of needles as described by Silk et al. [STS*14] is one such requirement. All needles placed in close proximity to a lesion need to be parallel to have the electric field equally applied to the designated area. Only by establishing this, an accurate prediction of the treatment zone becomes possible. As a conclusion, Silk et al. state: "More studies are needed to optimize device settings, probe positioning, and treatment parameters before IRE becomes more mainstream.". Another requirement is the correct relative depth of the used needles because the ablation area is limited by the overlap. Finally, the positioning pattern plays an important role in terms of the applied voltage and current between needles. These requirements are often challenging to meet during surgery, but the situation can become even more difficult based on the given context. For instance, structures like the rib cage or tissue to be penetrated by a needle can cause critical deviation or bending of a needle. This would result in an uneven and non-parallel arrangement of the needles.

In this paper, we present a novel visualization technique which is designed to display all crucial needle properties to meet the needle placement requirements consisting of parallelism, positioning, and depth. In this work, the focus lies on convex needle configuration patterns without probes passing through the center of a tumor. We aim at enhanced accuracy to reduce unnecessary vessel or tumor injuries and therefore decrease the risk of spreading tumor cells to surrounding tissue as well as prevent bleedings inside the organ. Furthermore, the visualization has been designed to enable fewer repositioning steps of needles when they are not in the correct place, as speeding this process

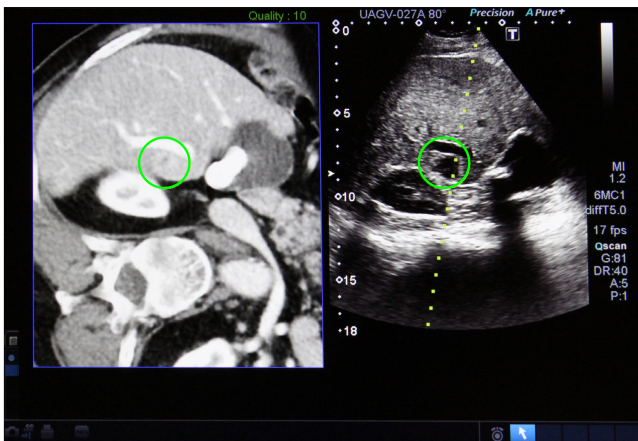


Figure 2: The surgeon places an IRE needle with the help of ultrasound (US) images as seen on the right. The needle is attached to the side of the US probe to have a first estimate where in the image it should appear (*green dotted line*). A live deformed CT scan of the patient with the marked target tumor (*green circle*) is displayed on the left.

up will benefit the patient. Additionally, enabling a more precise placement through visualization can help to reduce the number of CT scans required for placement verification. The results of our user study indicate that we could achieve these goals as the proposed visualization increases speed and accuracy during needle placement.

Additional information regarding the IRE intervention and related precautions can be found in the manual of the NanoKnife system, manufactured by AngioDynamics [Ang11]. We adapt the terminology in this paper from the work of Wendler et al. [WFR*16]. They propose a set of reporting criteria and terms for IRE procedures for analysis and comparison.

The paper is structured as follows. After having discussed related work in Section 2 we will describe the medical background of the IRE procedure in Section 3. In Section 4 we justify the design decisions made to develop the proposed visualization techniques and we discuss the application to real-world use cases in Section 5. Section 6 provides implementation details. Section 7 discusses the evaluation we have conducted together with three surgeons and provide the results of a performed user study. Limitations of our visualization are discussed in Section 8. Finally, we will conclude in Section 9 and summarize our results and findings the carried out study provides.

2. Related Work

The need for precise targeting in IRE and similar ablation modalities, as well as biopsy, has resulted in the development of various systems addressing this problem. Single targeting systems are useful in case of ablation techniques in which the spatial relations like parallelism or the distance between multiple tools are not relevant. Wallach et al. [WTW*14] compare three optical single targeting devices and conclude that the lateral error can be reduced significantly when using an aiming device over freehand insertions. A robotically assisted solution for tumor ablation in the liver is presented by Abdullah et al. [AYG*15] to render the probe placement independent of the physician's experience. Similar solutions have also been proven successful in other scenarios [GBG*14].

With the rise of Augmented Reality (AR), this technology will most likely also find its way into the surgery room [RBBS06], especially since much work has been done already in this field [BBR*03]. AR will increase targeting precision by enabling the surgeon to have a look inside the patient through superimposing content on the skin or even directly on organs [GAP*11]. Nicolau et al. present two AR navigation systems which can reach accuracy of 3mm on a phantom [NGP*05] and 5mm in real surgeries [NPS*09] in case of single needle targeting in a thermal liver ablation. An illustrative visualization for AR in liver surgery is suggested by Hansen et al. [HWR*10] with the goal to improve the spatial perception. To maintain the visual attention on the patient, Black et al. [BAIRH13] introduce auditory AR for needle placement. A context-aware augmented reality system is presented by Katić et al. [KWG*13] which supports surgeons through ontology-based situation interpretation and presentation.

Within the visualization community, ablation zone visualization for thermal treatment was done by Rieder et al. in multiple works [RAK*10, RKSH11]. Considering the patient's anatomy they present a fast image-based approximation of the ablation zone which takes the heat-sink effect into account [RAK*10]. They also show how a GPU-based approach approximates the ablation zone for different radio-frequency models using weighted distance fields [RKSH11]. Lehman et al. analyze the cooling effect of liver vessels on radio-frequency ablations and advise that in a range of 10 mm around major vessels this effect should be taken into account [LRV*09]. Kröger et al. present a FEM

based simulation of the ablation zone [KAP*06]. Other works in the area of visual liver surgery guidance, which traditionally requires high accuracy, include the analysis of the vasculature [SPSP02] or the development of complete pre-operative planning systems [BSL*02, MTC02]. Besides liver surgery, Neubauer et al. have shown that also endoscopic guidance can benefit from adequate visualizations [NMW*04].

Needle pathway planning is another field of application which tries to solve the problem of accessing targets in volumetric organs in the most appropriate way without damaging nearby structures. Khlebnikov et al. [KKMS11] visualize the safety of a path using crepuscular rays while Chan and Heng [CH14] propose an evaluation framework and an illustrative rendering technique to display needle access pathways using volumetric beams as depth and an array of rings as orientation cues for needles. Straight access paths in neurosurgical environments can be employed to render surface maps which represent the risk or safety potential when entering the brain at different locations [NTS*10, RNNTD14].

A different field for accurate navigation is deep brain stimulation (DBS). Bjartmarz and Rehncrona compared frame-based and frameless navigation for DBS electrode implantation and concluded that a conventional stereotactic frame performs better than a frameless guidance [BR07]. Bock et al. propose a visualization system which supports the surgeon during the placement of the stimulating electrodes with fused modalities like imaging data or patient checks [BLE*13].

While all of these approaches target higher accuracy in placement surgeries, no visualization-driven approach exists which takes into account position, parallelism, and depth of multiple needles in IRE interventions.

3. IRE Intervention Procedure

When performing IRE tumor treatment, the correct placement of the IRE needles is of great importance. Accordingly, intra-operative imaging techniques are applied to support the placement process. Currently, two imaging approaches are widely used: intra-operative CT scans and US probing during laparoscopic interventions. Prior to the actual placement, the surgeon plans how many needles are to be used and in which pattern they are placed according to a pre-operative CT scan of the tumor. In the following, two common workflows for IRE procedures are described.

CT-guided placement. If a CT scanner is used for placement verification, the IRE needles can be inserted using two different



Figure 3: Final IRE needle placement before the actual start of the ablation which takes several minutes. On the bottom our 3D model of an IRE needle with an adjustable exposure of the tip is shown, as it is used in our 3D visualization.

navigation approaches. Either through CT fluoroscopy or by exploiting computer-assisted guidance using jet ventilation to inhibit lung and liver motion and fusion of pre-operative scans to evaluate needle placements (see Figure 2). The IRE needles are initially inserted while they are attached to the side of an US probe to track them until they reach their target position around the tumor. Once a needle is in place, an intra-operative CT scan is performed and evaluated by the surgeons to verify if it is inserted as desired. Considered factors are the needles' parallelism, positioning with respect to the target tumor, depth in the tissue, and also the distance between needle pairs. These parameters need to be passed on to the ablation device which supplies the needed energy. Since the ablation area is in the centimeter range (0.5 cm to 4 cm), a correct insertion is crucial to the successful treatment. If indications exist that a needle has not been placed as expected, it will be removed completely and reinserted again. Another CT scan will then verify the placement until all parameters ensure a good ablation (see Figure 3).

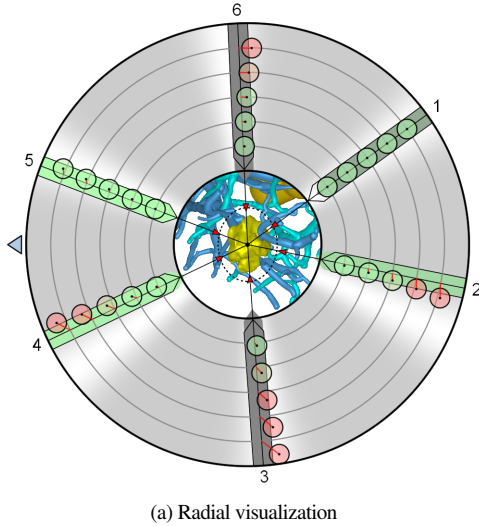
Laparoscopic placement. In the laparoscopic case, the needles are placed without an additional aiming device. Since the needle insertion is better stabilized with two fixed points (abdominal wall, then 5-8 cm of carbon dioxide filled void in the abdomen), before the needle enters the target organ (liver or pancreas), a guide arm is not used in this procedure. During the insertion, an US probe on the surface of the treated organ is used to track the needle inside the affected tissue until it is in the correct place. Due to the limited verification in the laparoscopic case, an additional visualization for guidance would be particularly beneficial here.

As two use cases exist in which the IRE method is applied, the CT case is primarily intended to be a post-placement check situation in which the placement itself is separated from the visualization process. The scan data can be analyzed and visualized to obtain a snapshot of the situation in the patient and to decide whether a correction is required. In the laparoscopic case, needles are tracked and can be integrated into our visualization during the insertion as an additional guidance in real time. We expect our visualization to be advantageous particularly during laparoscopy, as needles can be corrected in real time and a repositioning can be prevented early on in the process.

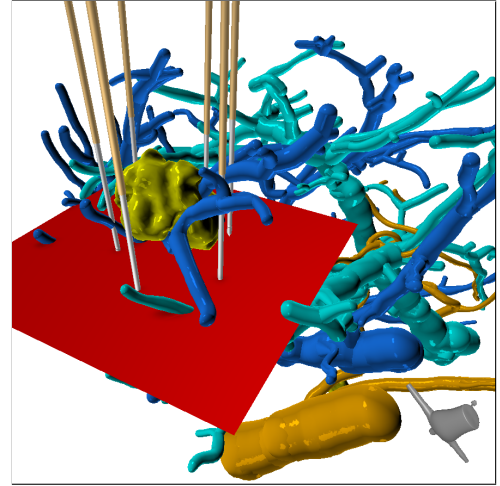
Therefore, the subsequently described placement phases focus on the laparoscopic case with the potential to facilitate an already acceptable result on the first try with interactive feedback of the proposed visualization. Thus, after the surgeon has chosen a placement template which defines the overall arrangement of the needles, we distinguish three subsequent phases in which certain parameters of the currently used needle are adapted: positioning, parallelism, and depth. As pointed out above, finding optimal values for all these parameters simultaneously is crucial and challenging. In particular, as the needles are bendable, no overall parallelism to a reference axis can be ensured along an entire needle.

4. Visualization Design

During the development of our visualization approach, we took into account the current IRE workflow as described in the previous section. Our visualization aims at displaying all relevant needle parameters – positioning, parallelism, and depth – simultaneously for multiple needles. This is achieved by facilitating a radial visualization which exploits reprojection in order to integrate these partially orthogonal parameters. Furthermore, it was important to integrate all these parameters into a single view to reduce focus changes. A single 3D view without further extensions would not be appropriate as demonstrated in Figure 1. In such a 3D view, for instance, needle depth and parallelism could not be conveyed simultaneously due to occlusion, as these are orthogonal parameters. The following subsections give an overview of the proposed visualization, discuss the underlying design choices, and



(a) Radial visualization



(b) Enhanced 3D visualization

Figure 4: Laparoscopic use case visualized with the proposed radial visualization (*left*) and the enhanced 3D visualization (*right*). In the radial visualization, needle number 1 is used to derive the reference axis a_{ref} . While the 3D visualization clearly allows to spot bad placement for some needles, it is not easily possible for all of them. Furthermore, the radial visualization communicates misplacement more accurately and also provides hints on what needs to be adapted.

explain how the displayed features help to determine optimal parameters. Finally, we discuss the visual complexity of the proposed visualization.

4.1. Radial Visualization Layout

Before we describe how the proposed visualization facilitates achieving values for the three placement parameters in the best manner possible – positioning, parallelism and depth – in the following subsections, we briefly explain and illustrate the coordinate system on which our radial visualization is based.

Reference coordinate system. It is essential to choose a common reference coordinate system to be able to integrate all relevant parameters into a single visualization. From now on we denote axes with small letters and their corresponding direction using vector notation, with x and \vec{x} as an example. Figure 5 illustrates the coordinate system used for our visualization. The main reference axis a_{ref} , and its direction \vec{a}_{ref} , can be chosen in two ways, depending on the surgeon’s preference. Either, as the average direction of all already placed needles, or a specific needle can be selected to serve as reference. The direction of the second axis \vec{a}_{head} is chosen to be in the plane spanned by a_{ref} and the direction from the center of the tumor c_{tumor} to the patient’s head, denoted by the vector \vec{g}_{head} . It is calculated to be perpendicular to \vec{a}_{ref} and pointing the same general direction using

$$\vec{a}_{head} = \vec{g}_{head} - \vec{a}_{ref} * (\vec{g}_{head} \cdot \vec{a}_{ref}) \Rightarrow \vec{a}_{head} = \frac{\vec{a}_{head}}{\|\vec{a}_{head}\|}$$

The third axis a_{orient} is obtained by calculating the cross product $\vec{a}_{ref} \times \vec{a}_{head}$. Consequentially, the plane in which the radial visualization is embedded is spanned by \vec{a}_{head} and \vec{a}_{orient} , positioned at the tumor center c_{tumor} . This is done to obtain a consistent view when looking at already placed needles from the direction of insertion due to the dependency on the patient’s position. To position this reference coordinate system in space, the target tumor’s center c_{tumor} is used as the origin. The direction of the patient’s head is depicted by means of a blue triangle (see Figure 4a) to support a quick orientation of the

surgeon. The arrangement of the needles in our visualization is conform to the surgeon’s view onto the patient when standing next to him and the patient is bedded with the head pointing in the same direction as the intended indicator (blue triangle). The same applies for a similar setup in a rendered 3D view. Furthermore, the 3D scene shows a small upper body in the lower right corner to provide an easy orientation (see Figure 4b).

Radial Layout. We use a radial shape as the global layout of the proposed visualization (see Figure 4a), because the arrangement template of IRE needles for small tumors is centered around the target in a convex manner. The radial visualization contains as many radial axes as needles there are used in the IRE process. Each axis represents all information required to allow for an optimal needle placement. The overall appearance of our radial visualization has been inspired by star glyphs [JFRH72]. Each axis is partitioned into several segments, which encode the essential information. As mentioned in Section 3, IRE needles are bendable and thus parallelism to a reference direction, which can also be illustrated or visualized as a reference needle, is not necessarily a global feature

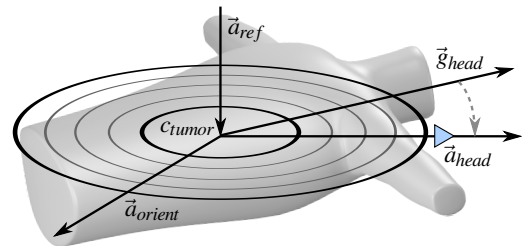


Figure 5: The radial visualization’s coordinate system is defined in the frame of the vectors \vec{a}_{head} and \vec{a}_{orient} centered at the target tumor’s position c_{tumor} . The head indicator (*blue triangle*) is used as a reference when aligning the radial visualization with the 3D scene, in which the patient is oriented along g_{head} .

but rather a feature of different segments. To cover such a potential bending of the needles, the axes of radial visualization are subdivided. The division is chosen such that it complies with the expected degree to which a needle can be bend. The location of the indicator point of each segment (small circles in Figure 4a) encodes the parallelism of the according segment. However, we deviate from the original star glyph design as we do not connect the neighboring axes, but rather offset the data points from the respective axis and depict the deviation from the optimum with a connection line. This gives us one more degree of freedom, which is necessary to encode needle bending in all directions. Keeping the number of segments low reduces the overlap between indicators which makes it more distinct where they need to be moved to during the guidance. In contrast, with a large number of segments, the bending of needles can be represented more accurately. How the indicators for these segments along the needle are distributed depends on the use case. However, the distribution along the needle's active area is meaningful to ensure optimal conditions for the ablation. Furthermore, the radial axes are used to encode a needle's insertion depth.

To support optimal needle targeting, we add an inner circle to the radial visualization, which displays relevant structures as seen from the surgeon's perspective. The proposed visualization combines two projections, for supporting optimal needle placement and simultaneously helping to avoid injuring important structures at the same time.

4.2. Encoding Positioning

Through the placement of the first needle during an IRE intervention, the surgeon defines the initial direction of insertion of all following needles. During the first phase of each needle's placement, the distance relation to the target tumor as well as to critical structures needs to be taken into account. To prevent the needle from harming vessels or other tumors, a certain security distance to them has to be ensured. Otherwise, possible consequences could be serious bleeding or a spreading of cancerous cells into other regions. Thus, a visualization supporting this first placement phase must consider two things. One is the currently inserted needle's distance to the arrangement template. The other would be the position of

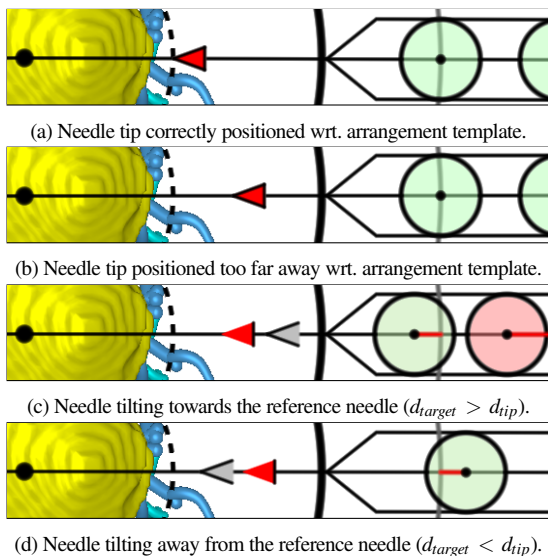


Figure 6: Examples of how the needle tip indicators (red and grey arrow) communicate the positioning and the tilt of an IRE needle.

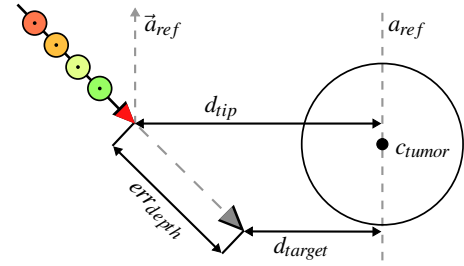


Figure 7: To encode correct positioning, the distances d_{tip} and d_{target} to a needle's tip are measured from the reference axis a_{ref} through the tumor's center c_{tumor} to the point of interest. Here, the red and the gray arrow correspond to the respective arrows in our radial visualization (see Figure 4a), where they denote the physical needle's tip position (red) and projected along the needle's direction to the target depth (gray). The segment indicators on the needle have a color assigned corresponding to the distance from a line through the current needle's tip (red) with the direction of the reference axis a_{ref} , denoted as \vec{a}_{ref} .

the needle when inserted to the final depth inside the tissue. We employ the inner circle of our radial visualization to encode these parameters.

The chosen arrangement template is displayed in the center of the inner region as a dashed line (see Figure 4a). In our current implementation, the arrangement template can have an elliptical shape. It serves as an easy to parameterize approximation of a convex polygon and is adjustable along its two principle axes. This kind of elliptical profile correlates to the appearance of a treated tumor in most cases. During the positioning phase, the surgeon must then place each needle's physical tip (represented by a red arrow) on the skin of the patient, such that it is aligned with the arrangement template (see Figure 6a). If the projection of the needle's tip onto the plane of the radial visualization is too far away or too close to the target tumor, it does not align with the arrangement template. Figure 6b illustrates such a case in which the tip is positioned too far away. Therefore, the surgeon can adjust the positioning before inserting the needle through the patient's skin. We also include an additional gray indicator, representing the needle's tip projected to its final position at the correct target depth. When viewed together, the red and gray indicators are additionally utilized to encode the tilt of needles, further explained in Subsection 4.4. An illustrative explanation on how we make use of the term *tilt* in this work is given in Figure 8.

To avoid positioning a needle where critical structures would be damaged upon insertion, the inner area of our radial visualization shows

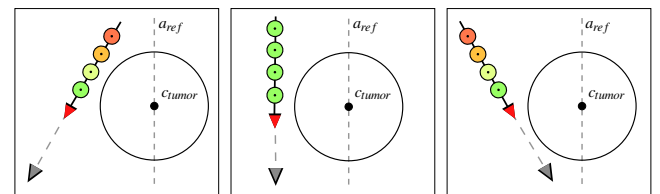


Figure 8: Three needles in different configurations relative to the reference axis a_{ref} . The general symbol notation is the same as in Figure 7. From left to right: a needle tilting towards a_{ref} , arranged parallel to a_{ref} , and tilting away from a_{ref} .

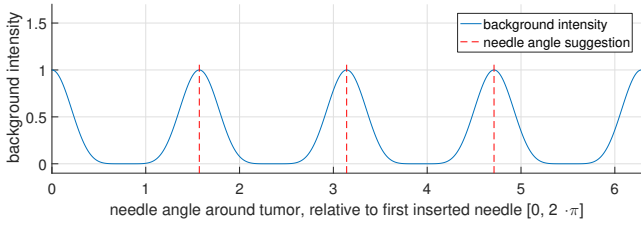


Figure 9: Background intensity used as a visual cue for suggesting needle distribution, in this case for four placed needles.

a projection of the underlying structures as seen along the reference axis a_{ref} . Since the distance calculations were done in the reference coordinate frame, our two arrow indicators are directly aligned with this geometry, such that they can be superimposed. Thus, an overlap between the red arrow indicator and a critical structure would signal an intersection of the needle and the structure when the needle is inserted along a_{ref} at this location.

4.3. Encoding Needle Distribution

Placing the needles in a uniformly distributed manner around the tumor provides a good coverage of the treated area. By optimizing the configuration, a minimum amount of needles can be used while remaining able to ablate all the malignant tissue. We incorporate a grayscale shading into the background of the outer part as a subtle hint to the surgeon (see Figure 4a). By avoiding a strict marker to indicate the placement, the surgeon is smoothly guided but not forced to place a needle close to critical regions. The shape of the effect can be adjusted to create wider or sharp highlights. In our case, we use a y -shifted *cosine* with the angle of the first inserted needle around the tumor as an offset parameter. The number of needles in total is used as the number of peaks. An additional exponent to the cosine controls the sharpness of the effect. As an alternative to the cosine, one could think of using a sigmoid function to create a smooth ascending and descending shape. Of course, a manual adjustment of the pattern's arrangement is also possible at all times if a surgeon is not satisfied with the presented configuration. Figure 9 shows a simple example of how the background color intensity could look like in the case of four placed needles.

4.4. Encoding Parallelism

In the second phase of a needle's placement, the instrument needs to be oriented such that it is parallel to the reference needle direction \vec{a}_{ref} . We identified three reasons which make multiple encodings for needle parallelism in our visualization necessary. First, as parallelism is the most crucial of the needle parameters, an unambiguous communication is essential. Second, as the needles are bendable, parallelism must be encoded for several segments along a needle. Third, to gain an estimation of how a non-parallel needle can be corrected, it is necessary to communicate how a needle deviates from a parallel path. We use an explicit coding for parallelism. It encodes in which direction a segment is deviating from its neutral position on the corresponding radial axis. Instead, implicit coding would map parallel structures of the object to parallel structures in the visualization. Forcing parallel needles in the 2D plot as well would require a second view to be able to recognize a tilt in all directions. A visualization of parallelism based on one visual element instead is easier to quantify.

To recall the two arrow-shaped needle tip indicators introduced in Subsection 4.2, a first impression of a needle's tilt with respect to the reference axis a_{ref} is already provided in the positioning phase. We have previously experimented with cross hairs. The choice of an arrow as the target structure has the advantage that it perfectly matches the red arrow when the needle is pointing in the same direction as the current reference axis a_{ref} which indicates that the needle follows a parallel path with respect to a_{ref} towards the target (see Figure 6a and 6b). Otherwise, the needle is tilted either inwards (see Figure 6c) or outwards (see Figure 6d). To correctly display the two arrow markers representing the needle's tip, we have to compute their position with respect to the inner circle. We refer to these values as the current tip's position d_{tip} and the position in which the tip would hit the target plane d_{target} . They are both measured from the current reference axis a_{ref} through the tumor's center c_{tumor} as illustrated in Figure 7.

To allow for communicating parallelism of bendable needles, we exploit the multiple segments along the radial axes. When orienting the currently inserted needle parallel to a_{ref} , all segments have the same distance to its corresponding pair along the reference. An example of such a setup can be seen in Figure 10a, where all segment indicators, depicted by the green circles, are perfectly aligned along the needle and the concentric circles on our radial visualization. This resembles a cross hair metaphor which is known to be a sufficient guidance system in similar application cases [GFA*12]. If a needle is not parallel, two scenarios can occur. First, the needle is tilted towards or away from a_{ref} resulting in potentially different angles for different needle segments. Having the tip as the reference point, this error can be visually communicated through the segment indicators moving along the needle's axis towards or away from the center, depending on the tilt direction (see Figure 10b and 10c). Second, the segments can also rotate around the reference coordinate frame's main axis a_{ref} . This angle error is shown by the

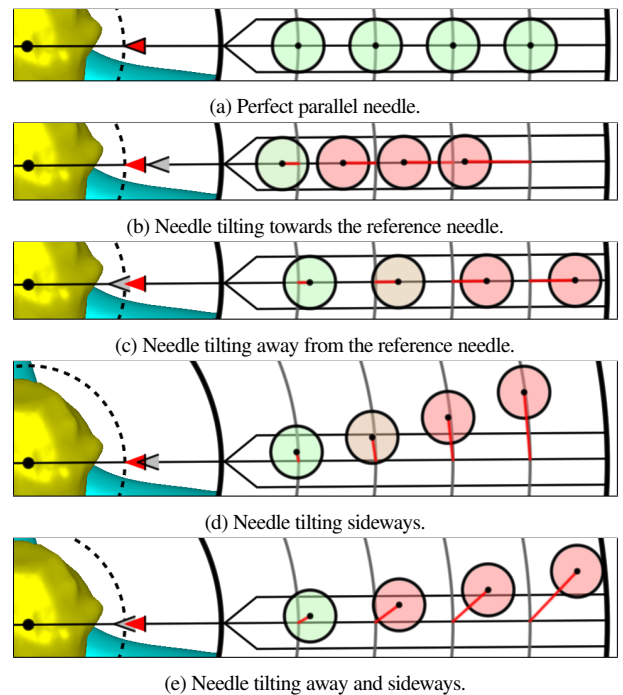


Figure 10: Examples of different situations while adjusting the parallelism of a needle wrt. to the reference axis a_{ref} .

segment indicator as a rotation away from the needle's axis in our radial visualization (see Figure 10d). Indeed, the two directions of rotation can be combined for a single needle. Such a setup is depicted in Figure 10e. The tilt towards or away as well as sideways from the reference needle can also be imagined as the azimuth and elevation angle on a spherical coordinate system. These two quantities are two-dimensional and therefore suitable to be displayed on a plane. The amount of movement the needle experiences during manipulation correlates to the position of the segment on the needle. The closer it is to the needle's tip, the smaller the deviation of the segment. The color gradient from green to red represents an increasing distance error from the reference line through the needle's tip with the direction \vec{a}_{ref} of the reference axis as can be seen in Figure 7.

Multiple visual cues are again used in order to allow for an easy correction of non-parallel needles. First, a red connection line indicates where the optimal position for each segment indicator would be. Second, the color of the indicator changes from red to green when coming close to this optimal position. This color transfer can be adjusted to have a specific threshold in distance and angle error from the optimum to ensure a good ablation if a tolerated error is known. A third cue is based on the alignment of the dot in the center of the segment indicator with the optimal position, which is represented by the intersection of the needle's axis and the segment's concentric circle. At last, we have chosen the width of the segment indicator to be the same as the width of the box-like needle abstractions around the axes. This helps to correct the angle error, as when both align, the targeting circle is exactly within the bounds of the needle abstraction.

4.5. Encoding Depth

During the third and last phase, a needle is inserted until it reaches the target depth around the tumor in order to place the active tip in the planned treatment zone. Since the depth range of a typical treatment zone is quite small (0.5 cm to 4 cm), accurate depth positioning is important. For instance, if the target tumor is located close to major vessels or other tumors in the same area, going further down than needed would be a risk that should be avoided. While the needles themselves have length markers, as can be seen in Figure 3, they may differ in depth due to bending caused by tissue or structures on the way towards the target location. Thus, we have incorporated a visualization of the needle's depth in our radial visualization.

The considered depth which has to be advanced is the offset from the target plane as viewed along the currently placed needle, and not along the reference axis direction \vec{a}_{ref} (see Figure 7). Although all

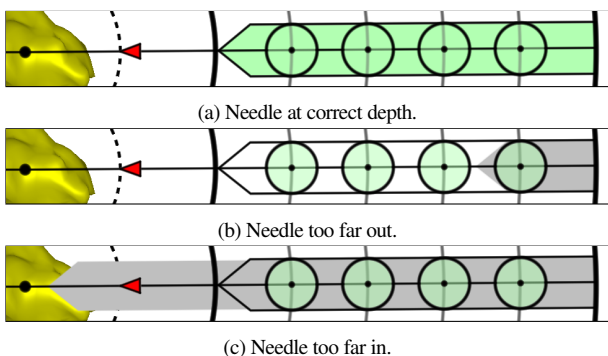


Figure 11: Examples of how the depth indicator communicates the distance of a needle's tip from the target depth.

previously described phases achieve already a good parallelism, this depth measurement is done to obtain the accurate depth which the needle needs to be placed in the tissue. The visual representation of this depth is incorporated in the rendered needle abstraction as shown in Figure 11. During the insertion process, we fill the needle representation from the outside with another box-like needle representation in gray. When the needle comes close to the target depth, the color will blend to green in order to signify a correct positioning. While Figure 11a shows such a correct positioning, Figure 11b and Figure 11c show the representation of a needle that is too far out or in, respectively.

To complement this information, the current target plane can be shown in the 3D visualization (see Figure 4b) to provide a second depth confirmation. Despite the fact that this is not a quantitative representation like our depth indicator as it depends on the viewing angle, it gives a first impression of whether the setup looks acceptable as needles piercing through this target plane can be quickly identified.

4.6. Needle Correction

With the coordinate system set up as explained earlier in Subsection 4.1, surgeons can correct a needle directly based on the radial plot. While placing a needle, all manipulations performed resemble the changes in our visualization when the head indicator (blue triangle) is aligned with the patient's head direction from the surgeon's point of view. For instance, moving the needle left or right on the patient's skin surface moves the needle's tip indicator (red triangle) to the left or right respectively. The same applies for tilting the needle. A tilt towards the reference axis \vec{a}_{ref} moves all segment indicators closer to the center of the radial plot and vice versa.

4.7. Visual Complexity

The size and amount of the segment indicators is a trade-off between a good representation of the bending behavior and not ending up with an overloaded area. Having the segment indicators large enough is required to be able to see the target dot in the middle for the alignment with the corresponding concentric circle. We have chosen five segment subdivisions in our example since at least two are needed to capture the bending. Five elements, in the end, had still sufficient spatial separation to clearly identify which indicator belongs to which target position. We chose the radius of the inner area to be twice as large as the major axis of the ellipse for the positioning template. This is done to leave space for the distance indicator to be seen while targeting for the correct spacing to the tumor. The 3D rendering in the middle of the plot is scaled accordingly. The ratio between the inner and outer area is chosen dependent on the number of segments displayed along the needle. Fewer segments allow a larger inner area and vice versa. Each segment is uniformly distributed along the whole active part of the needle.

5. Use Cases

In this section, we describe how our visualization is applied to the CT and laparoscopic placement use cases introduced in Section 3.

5.1. Laparoscopic Interventions

The main surgery technique where our visualization technique is beneficial for IRE ablation is the laparoscopic case. Here surgeons are limited to the in-organ images provided by an US probe, work without mechanical guidance and do not have a complete overview of all placed needles simultaneously.

In order to improve the placement in this situation, our system supports tracked needle data from different sources, such as optical or electromagnetic tracking or US image analysis. Thus, the needle position and orientation is taken into account together with all calibration data needed to register the used tools to the system. Together with segmented anatomy provided as mesh data, a real-time visualization is possible where our radial visualization displays the currently tracked needle as guidance to its optimal position through all the three phases described above. To complement this visualization with a view familiar to the surgeons, a 3D view with the anatomy data as well as models of all tracked needles is provided. In this view, surgeons can freely move around and observe the situation.

5.2. Intra-Operative CT Scans

IRE ablation with the use of a CT scanner is the second surgery case in which our visualization can be applied. While in this situation a real-time tracking system is not available in the surgery room, the intra-operative CT scans acquired after each needle placement can be automatically analyzed. Therefore, we have extracted the needles from the CT scan in an automated process. To do so, we first apply a transfer function to the data which separates all metal objects and structures with a similar density from the rest of the patient's body. This first segmentation is then used to analyze slices of the volume roughly along the needles' major insertion direction. Stepping through the volume as long as the needles are visible in the segmented slice, a blob detector can identify the 2D locations of the needles in the slice which can be transformed back into a 3D location. This results in line strips used to take samples along the needles from which our radial visualization can be calculated. The average of the needles' tips is used for the target plane's location. Figure 12 shows the application of our IRE visualization to a CT use case.

6. Implementation

To obtain the visual results presented in this paper, we implemented all described techniques on the GPU. Thus, we were able to achieve high-quality results while at the same time maintaining interactive

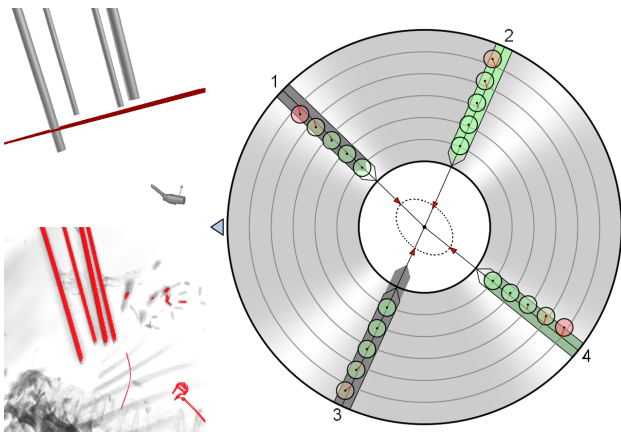


Figure 12: Application of our visualization to a CT use case. The three views show a CT volume rendering (*lower left*), a 3D view with the automatically extracted needles and the target plane (*upper left*), and our radial visualization communicating needle positioning, depth and parallelism (*right*).

frame rates. In the following paragraphs, we describe how the radial visualization and the used 3D views have been implemented.

Radial visualization. As accuracy is crucial for our application, we chose that the visualization should be comprised out of well defined shapes which are image resolution independent. Therefore, when rendering shapes like points, line segments, circles, ellipses, or convex polygons, we avoided the rasterized polygon approach and facilitated analytic rendering of signed distance functions using a single fullscreen quad shader instead. The main motivation to do so was the fact that our radial plot mostly consists out of circular shapes which can be evaluated very easily and accurately using an analytical approach. Thus, we determine every pixel's color based on its distance to the surrounding elements. In this manner, effects like line thickness, a soft edge falloff, dotted lines, color blending or transparency can also be easily implemented with anti-aliasing automatically embedded.

3D visualization. A multi-layer BRDF is used for the 3D view to render all internal structures of the liver such as vessels and tumors. The Oren-Nayar reflectance model is used for the diffuse reflection and the Cook-Torrance model for the specular component. Additionally, we apply horizon-based ambient occlusion [BS09] to the final rendering for enhanced shape separation and depth perception.

7. Evaluation

In order to evaluate our visualization, we examined the system together with surgeons performing IRE treatments. Additionally to this qualitative survey, a user study was conducted to identify advantages and disadvantages. We measured the users task precision and completion time.

Prior to the actual user study, a pilot study was performed which revealed a drawback of our original visualization scheme: The needles' distribution around the tumor was hard to determine. Therefore, the feature described in Subsection 4.3 was incorporated.

7.1. Qualitative Evaluation

In order to better understand the challenges during an IRE surgery, we attended three operations live in a surgery room. One IRE patient was treated under a CT scanner with an US probe placement. In the other two procedures, the current guidance system was used in a CT and laparoscopically for thermal ablation but with the same equipment as the IRE would have been performed with. Based on this experience we set up a qualitative evaluation to investigate the usefulness of the developed visualizations after the development process has been finished.

Study setup. While the presented visualization method was designed in close collaboration with one surgeon who frequently performs IRE interventions, we wanted to investigate its usability with respect to real-world cases from the perspective of multiple surgeons. Therefore, we have evaluated the proposed visualizations with three experienced surgeons. The surgeons included in the study have a cumulative experience in IRE treatment of several decades. They started performing IRE interventions in February 2014, and have since then treated 27 patients, of which 3 were pancreas and 24 were liver cases. Due to the fact that technology used in the surgery room needs a medical certification, we could unfortunately not apply the presented visualization during the intervention. Instead, we have performed a twofold evaluation. First, we have introduced and explained the visualization to the surgeons during a live session in a laparoscopic setup lasting about 30 minutes.

Second, to assess the usability in the CT guidance setup, we have additionally confronted the surgeons with 9 images showing our visualization applied to liver surgery cases, they have performed earlier

in the same week. While we have taken live feedback during the introduction session, the feedback regarding the CT guidance was collected via email, as immediate access to the patient's CT scan data while we attended the surgery was not allowed. Specifically, we have asked the following questions: *'Is the volume rendering alone (or CT slices, as you are used to use) more helpful than the radial visualization together with the extracted needles and the target plane?'*, *'Which needles would you place again or adjust and why?'*, *'Is the overall bending of the needles a distraction from the actual important needle segment at the tip?'*, and *'Is the comparison against a specific reference needle more helpful than the comparison against the average?'*

Study feedback. Regarding the laparoscopic case study, we retrieved very positive feedback from the surgeons. They made statements like *'very nice'*, that they were *'impressed by the precision'* and that they see our visualization as a *'helpful tool for judging parallelism'*. One was stating, that *'the radial visualization will shine in a laparoscopic [...] setting where direct imaging is not possible'*. However, they also pointed out that they would like to see it live, as then you will see *'how well you can align it with this visualization'*. Based on their feedback and the interchange of some thoughts and ideas afterwards, we conclude that for laparoscopic surgeries our visualization technique could have a significant impact. Especially, since US imaging cannot provide a good enough overview of the needle setup as a whole and can't capture multiple needles simultaneously. Thus, checking the spatial relations between needles becomes a difficult task when the number of needles increases. According to the surgeons, having support by visualization will presumably benefit laparoscopic surgeries, since currently a validation cannot be done for all needles simultaneously.

Unfortunately, for the CT cases, the surgeons were less positive about the radial visualization. First of all, only one out of three replied to our questions regarding the recently performed surgery, while for the laparoscopic case study we got feedback from all of them. The tenor of the answers was, that for the CT situation the volume rendering with the target plane (as shown in Figure 4b) is already *'quite intuitive and provides sufficient visual data, especially if the tumor would also be visible'*. However, based on the presented visualization, the answering surgeon was able to judge that he *'would retract the most lateral needle which is inserted a little too much'*, and said that the depiction of the overall bendings *'is not distracting'*. He also pointed out that *'using one reference needle is better, as if one deviates it is only that one that needs to be repositioned and it's error is better visualized against one reference needle than against the average of all four'*. Based on the feedback and further discussions, we conclude that the presented radial visualization is less useful for the CT cases. The main reason seems to be, that a needle is not inserted step-by-step during live imaging, but that a CT scan is acquired with all needles, which renders defining a reference direction and correcting single needles more difficult. However, the automatic needle extraction and the vicinity visualization with the ambient occlusion technique along the target plane was judged as helpful.

Identified limitations. Based on our subsequent discussions with the surgeons, we have also identified the following limitation. When a lesion is larger than the maximum size of the planned treatment zone in a convex pattern, a center needle is inserted directly into the tumor to broaden the coverage. This means that the risk spreading tumor cells exists but at least larger lesions can be dealt with. This obviously limits our visualization technique which is designed for needle placement around a target. However, this could be solved by considering only a subset of needles and ensuring their correct placement relative to each other. Having two subsets which cover all placed needles and have a large enough overlap, we hope in the future an acceptable result, in that case, can be achieved.

7.2. Quantitative Evaluation

We evaluated our visualization in a user study in which we compare two configurations. As the proposed visualization is meant to be an extra guidance, one resembles the currently performed procedure with the help of a 3D view (denoted as "3D" in following symbols and figures) and the other with the additional support of our radial visualization (denoted as "2D+3D" in following symbols and figures). We designed the study as within-subject. Every participant performed both tasks counterbalanced using Latin square, half of the participants started without and the other half with use of the radial visualization. 12 study participants (computer science students, of which 10 were male and 2 female) conducted the evaluation of our system, aged 24-37 with an average of 30. As all available surgeons contributed to the design of our visualization, they could not take part. Nevertheless, the task of judging needle attributes such as parallelism, position, and depth does not require medical domain knowledge.

Study task. The scenario we put the participants into was the placement of five needles around a tumor. The focus of the task was clearly stated to make the most out of their capabilities and not see the time as the main measurement parameter. Therefore, removing a needle and reinserting it was allowed to correct for an improved configuration and more successful ablation.

Study setup. To simulate a patient body in which to place the needles, a bucket of moist sand was on a table together with a rigid wooden needle. The sand made it possible to easily insert needles while also stabilizing them after letting go, which avoided late correction after needle insertion. A clean setup after each run could also be guaranteed. The removal of holes created by previous insertions was ensured. Markers attached to the needle and the table allowed for an optical tracking of the tool in relation to the virtual tumor inside the bucket. The assumption of a rigid needle was necessary to be able to correctly predict the position of the tool in space.

Participant introduction. Before the performance of the described task, our visualization was explained to every participant to make sure it was correctly interpreted. A short demonstration was performed to exemplify the behavior of the visualization when moving and tilting a needle. To familiarize themselves with the needle guidance and tracking, each participant placed a needle into the sand as a short training phase.

Study execution. In both setups, the participants had to verify and confirm the needles' placement around the target tumor. To facilitate

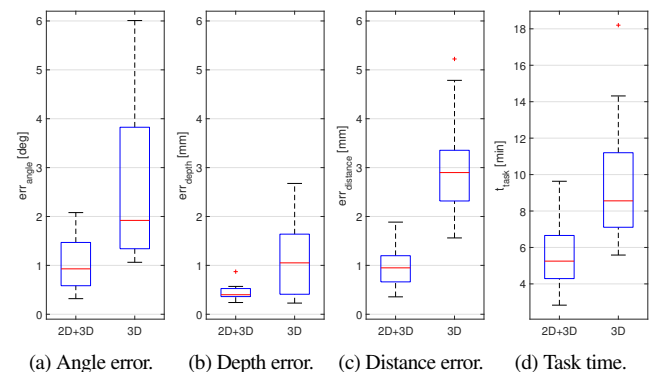


Figure 13: The pairs of box plots show the results of the performed study on the left side with use, and on the right side without use of the radial visualization.

this verification in the 3D view, the users could change the virtual camera at will. In the 2D+3D task they also had the option to change the virtual camera in the 3D view, but here no participant made use of this. We avoided a constant task switch between needle positioning and camera movement. Therefore, the camera of the 3D scene was navigated by an assistant to satisfy the participants desired view of the environment to perform corrections with the tracked tool.

Significance. When the participant was of the opinion that further needle repositioning would not benefit the current configuration anymore, all distance and angle measurements as well as the required task execution time were saved for later analysis. Since all participants performed both cases, we use the *Wilcoxon Signed-Rank Test* which is a non-parametric test for dependent samples to measure significant differences in the absolute error values. We compare the absolute error values for parallelism ($Mdn_{2D+3D}=0.92deg$, $Mdn_{3D}=1.92deg$, $W=4$), distance ($Mdn_{2D+3D}=0.95mm$, $Mdn_{3D}=2.90mm$, $W=0$), depth ($Mdn_{2D+3D}=0.40mm$, $Mdn_{3D}=1.05mm$, $W=6$) and additionally the task time ($Mdn_{2D+3D}=5.25min$, $Mdn_{3D}=8.56min$, $W=4$) as depicted by the box plots shown in Figure 13. For all measured variables, the differences were significant at $p < 0.01$.

System Usability Scale (SUS). We investigated the usability and learnability of our visualization using the SUS, proposed by Brooke et. al [B*96], to survey the participants after each task of the performed study. The overall SUS scores ($Mdn_{2D+3D}=82.5$, $Mdn_{3D}=42.5$, $W=66$) support our hypotheses as seen in Figure 14. We tested the significance similarly to the error measurements with a resulting $p < 0.001$. Most of the qualitative feedback we received from the participants indicated that the parallel and equidistant needle placement problem was much easier to grasp in our 2D visualization compared to the 3D view. A lot of them agreed that the control over the parameters was more intuitive and a satisfactory configuration was easy to find.

Study Conclusion. The evaluation of the study supports our hypothesis that a simplification from 3D to 2D in parallel needle placement can benefit accuracy and duration time. Achieving a parallel needle setup is an exhausting task using a single 3D view. A constant rotation of the camera is needed to be able to track the needles' orientation during the insertion process. Tilting can hardly be detected when the image plane is perpendicular to the deviation direction. With both tilt angles under observation, corrections can be recognized quickly.

Placing the needle at the correct depth was the most precise parameter the users could adjust. Compared to the error in distance to the tumor, regulating the depth of the needle requires only a single view of the scene.

Even if the difference in distance precision is the most prominent, this finding needs to be interpreted carefully. In a 3D view, lengths can only be estimated relative to other objects. Without a scale, only a rough estimate is possible. With our visualization, the user was able to refrain from relative distance estimations and end up with a more precise result.

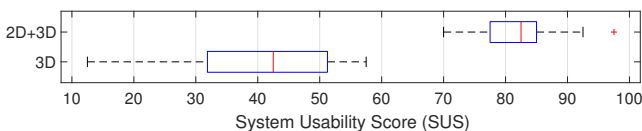


Figure 14: The result of the System Usability Score (SUS) questionnaire shows a clear tendency towards our visualization. This can be an indicator for a significant lower learning curve.

In our scenario, we were able to achieve a reduction in task duration by 42%. It is clear that under surgery conditions the overall procedure takes much longer and is more complex. However, we hope an improved placement process can save a lot of time by reducing task complexity and bring the surgeon more control over how the needles are inserted.

8. Limitations

Although we did our best to design the proposed visualization to support IRE interventions in the best manner possible, we are aware of some limitations. First, the placement pattern of IRE needles can exhibit one or multiple needles in the center of the ablated tumor which can not be represented by our approach. One possible solution, as already mentioned in Section 7.1, would be the utilization of multiple, circular subsets of needles in such a configuration which feature a large enough overlap to ensure an overall acceptable placement.

Second, the number of needles is ultimately limited. While we demonstrate a configuration of six needles in Figure 4a, there will be an upper limit before our visualization appears overloaded with information and overlap between visual elements will occur.

Third, the suggestion of the needle distribution (Subsection 4.3) is not dependent on the anatomical structures present. An automated optimization process where to insert needles would make it easier for surgeons to find an applicable configuration for the ablation.

Finally, internal tracking of all needles is necessary to make full use of our visualization. While after a CT scan the trajectory of all needles can be easily determined, the laparoscopic case relies on US imaging only which can not capture all needles at once. With an external, rigid tracking approach, bending can not be represented. In contrast to US-based tracking, electromagnetic tracking is currently not able to track a needle's tip as it is too thin to embed the sensor. Therefore, as IRE currently has to rely on imaging techniques such as CT and US, we see also many opportunities to include the imaging results with our visualization, for instance, to show the context or live US imagery.

9. Conclusions and Future Work

In this paper we have introduced a radial visualization which has been designed to support IRE interventions. The presented visualization has been developed to meet the needs of IRE procedures, such that it presents all data relevant to the surgeon in order to achieve an optimal needle placement. In contrast to previous approaches, the presented technique is the first visualization technique, which takes into account multiple needles, and thus does not only allow for optimizing parameters for single needle placements, such as position and depth, but also global properties such as parallelism. By combining two projections within an inner and an outer radial layout, we are able to visually convey parallelism, as well as needle depth and positioning in an intuitive manner without overloading the visualization. We have discussed the underlying design decisions, the implementation of the presented visualization, and we have evaluated the presented visualization with three surgeons. A quantitative evaluation also was performed in order to compare the performance with and without our additional visualization.

While the real-world use cases discussed in this paper focus on liver ablations only, IRE is also applied to pancreas, prostate and kidney tumors, three areas where we see potential for the introduced visualizations. In the future, we would like to investigate these application areas more closely. Furthermore, we aim at studying the usability in greater detail, first on phantoms, and then in the surgery room. We are confident that such studies would confirm the identified benefits of our visualization when it is used interactively.

References

- [Ang11] ANGIODYNAMICS: NanoKnife® system procedure & troubleshooting guide, version 2.20, 2011. 2
- [AYG*15] ABDULLAH B. J. J., YEONG C. H., GOH K. L., YOONG B. K., HO G. F., YIM C. C. W., KULKARNI A.: Robotic-assisted thermal ablation of liver tumours. *European radiology* 25, 1 (2015), 246–257. 2
- [B*96] BROOKE J., ET AL.: Sus-a quick and dirty usability scale. *Usability evaluation in industry* 189, 194 (1996), 4–7. 10
- [BAIRH13] BLACK D., AL ISSAWI J., RIEDER C., HAHN H. K.: Enhancing medical needle placement with auditory display. In *Mensch & Computer* (2013), pp. 289–292. 2
- [BBR*03] BORNIAK A., BEICHEL R., REITINGER B., GOTSCHULI G., SORANTIN E., LEBERL F. W., SONKA M.: Computer-aided liver surgery planning: an augmented reality approach. In *Medical Imaging 2003* (2003), International Society for Optics and Photonics, pp. 395–406. 2
- [BLE*13] BOCK A., LANG N., EVANGELISTA G., LEHRKE R., ROPINSKI T.: Guiding deep brain stimulation interventions by fusing multimodal uncertainty regions. In *Visualization Symposium (PacificVis), 2013 IEEE Pacific* (2013), IEEE, pp. 97–104. 3
- [BR07] BJARTMARZ H., REHNCRONA S.: Comparison of accuracy and precision between frame-based and frameless stereotactic navigation for deep brain stimulation electrode implantation. *Stereotactic and functional neurosurgery* 85, 5 (2007), 235–242. 3
- [BS09] BAVOIL L., SAINZ M.: Multi-layer dual-resolution screen-space ambient occlusion. In *SIGGRAPH 2009: Talks* (2009), ACM, p. 45. 8
- [BSL*02] BOURQUAIN H., SCHENK A., LINK F., PREIM B., PRAUSE G., PEITGEN H.-O.: Hepavision2—a software assistant for preoperative planning in living-related liver transplantation and oncologic liver surgery. In *CARS 2002 Computer Assisted Radiology and Surgery*. Springer, 2002, pp. 341–346. 2
- [CH14] CHAN W.-Y., HENG P.-A.: Visualization of needle access pathway and a five-dof evaluation. *IEEE journal of biomedical and health informatics* 18, 2 (2014), 643–653. 3
- [GAP*11] GAVAGHAN K. A., ANDEREGG S., PETERHANS M., OLIVEIRA-SANTOS T., WEBER S.: Augmented reality image overlay projection for image guided open liver ablation of metastatic liver cancer. In *Workshop on Augmented Environments for Computer-Assisted Interventions* (2011), Springer, pp. 36–46. 2
- [GBG*14] GERBER N., BELL B. J., GAVAGHAN K. A., WEISSTANNER C., CAVERSACCIO M., WEBER S.: Surgical planning tool for robotically assisted hearing aid implantation. *Int. J. Computer Assisted Radiology and Surgery* 9, 1 (2014), 11–20. 2
- [GFA*12] GAVAGHAN K. A., FUSAGLIA M., ANDEREGG S., PETERHANS M., WEBER S.: An evaluation of image overlay projection guidance for liver tumor targeting. In *CURAC* (2012), pp. 9–12. 6
- [HWR*10] HANSEN C., WIEFERICH J., RITTER F., RIEDER C., PEITGEN H.-O.: Illustrative visualization of 3d planning models for augmented reality in liver surgery. *International journal of computer assisted radiology and surgery* 5, 2 (2010), 133–141. 2
- [JFRH72] JH S., FARRELL E., RM G., HP F.: The surgical implications of physiologic patterns in myocardial infarction shock. *Surgery* 72, 1 (1972), 126–141. 4
- [KAP*06] KRÖGER T., ALTROGGE I., PREUSSER T., PEREIRA P. L., SCHMIDT D., WEIHUSEN A., PEITGEN H.-O.: Numerical simulation of radio frequency ablation with state dependent material parameters in three space dimensions. In *Medical Image Computing and Computer-Assisted Intervention—MICCAI 2006*. Springer, 2006, pp. 380–388. 2
- [KKMS11] KHLBNIKOV R., KAINZ B., MUEHL J., SCHMALSTIEG D.: Crepuscular rays for tumor accessibility planning. *IEEE transactions on visualization and computer graphics* 17, 12 (2011), 2163–2172. 3
- [KWG*13] KATIĆ D., WEKERLE A.-L., GÖRTLER J., SPENGLER P., BODENSTEDT S., RÖHL S., SUWELACK S., KENNGOTT H. G., WAGNER M., MÜLLER-STICH B. P., ET AL.: Context-aware augmented reality in laparoscopic surgery. *Computerized Medical Imaging and Graphics* 37, 2 (2013), 174–182. 2
- [LRV*09] LEHMANN K. S., RITZ J., VALDEIG S., KNAPPE V., SCHENK A., WEIHUSEN A., RIEDER C., HOLMER C., ZURBUCHEN U., HOFFMANN P., ET AL.: Ex situ quantification of the cooling effect of liver vessels on radiofrequency ablation. *Langenbeck's Archives of Surgery* 394, 3 (2009), 475–481. 2
- [LTK10] LEE E. W., THAI S., KEE S. T.: Irreversible electroporation: a novel image-guided cancer therapy. *Gut and liver* 4, Suppl 1 (2010), 99–104. 2
- [Mac01] MACK M. J.: Minimally invasive and robotic surgery. *JAMA* 285, 5 (2001), 568–572. 1
- [MILR07] MAOR E., IVORRA A., LEOR J., RUBINSKY B.: The effect of irreversible electroporation on blood vessels. *Technology in cancer research & treatment* 6, 4 (2007), 307–312. 2
- [MTC02] MEINZER H.-P., THORN M., CÁRDENAS C. E.: Computerized planning of liver surgery - an overview. *Computers & Graphics* 26, 4 (2002), 569–576. 2
- [Nar11] NARAYANAN G.: Irreversible electroporation for treatment of liver cancer. *Gastroenterology & hepatology* 7, 5 (2011), 313. 1
- [NGP*05] NICOLAU S., GARCIA A., PENNEC X., SOLER L., AYACHE N.: An augmented reality system to guide radio-frequency tumour ablation. *Computer animation and virtual worlds* 16, 1 (2005), 1–10. 2
- [NMW*04] NEUBAUER A., MROZ L., WOLFSBERGER S., WEGENKITTL R., FORSTER M.-T., BUHLER K.: Steps—an application for simulation of transphenoidal endonasal pituitary surgery. In *Visualization, 2004. IEEE* (2004), IEEE, pp. 513–520. 3
- [NPS*09] NICOLAU S., PENNEC X., SOLER L., BUY X., GANGI A., AYACHE N., MARESCAUX J.: An augmented reality system for liver thermal ablation: design and evaluation on clinical cases. *Medical Image Analysis* 13, 3 (2009), 494–506. 2
- [NTS*10] NAVKAR N. V., TSEKOS N. V., STAFFORD J. R., WEINBERG J. S., DENG Z.: Visualization and planning of neurosurgical interventions with straight access. In *International Conference on Information Processing in Computer-Assisted Interventions* (2010), Springer, pp. 1–11. 3
- [RAK*10] RIEDER C., ALTROGGE I., KRÖGER T., ZIDOWITZ S., PREUSSER T.: Interactive approximation of the ablation zone incorporating heatsink effects for radiofrequency ablation. In *CURAC* (2010), pp. 9–12. 2
- [RBBS06] REITINGER B., BORNIAK A., BEICHEL R., SCHMALSTIEG D.: Liver surgery planning using virtual reality. *IEEE Computer Graphics and Applications*, 6 (2006), 36–47. 2
- [RKSH11] RIEDER C., KRÖGER T., SCHUMANN C., HAHN H. K.: GPU-Based Real-Time Approximation of the Ablation Zone for Radiofrequency Ablation. *IEEE Transactions on Visualization and Computer Graphics (Proceedings Visualization 2011)* 17, 12 (December 2011), 1812–1821. 2
- [RNNTD14] RINCÓN-NIGRO M., NAVKAR N. V., TSEKOS N. V., DENG Z.: Gpu-accelerated interactive visualization and planning of neurosurgical interventions. *IEEE computer graphics and applications* 34, 1 (2014), 22–31. 3
- [SPSP02] SELLE D., PREIM B., SCHENK A., PEITGEN H.-O.: Analysis of vasculature for liver surgical planning. *Medical Imaging, IEEE Transactions on* 21, 11 (2002), 1344–1357. 2
- [STS*14] SILK M., TAHOUR D., SRIMATHVEERAVALLI G., SOLOMON S. B., THORNTON R. H.: The state of irreversible electroporation in interventional oncology. In *Seminars in interventional radiology* (2014), vol. 31, Thieme Medical Publishers, pp. 111–117. 2
- [WFR*16] WENDLER J. J., FISCHBACH K., RICKE J., JÜRGENS J., FISCHBACH F., KÖLLERMANN J., PORSCH M., BAUMUNK D., SCHOSTAK M., LIEHR U.-B., ET AL.: Irreversible electroporation (IRE): standardization of terminology and reporting criteria for analysis and comparison. *Polish journal of radiology* 81 (2016), 54. 2
- [WTW*14] WALLACH D., TOPOREK G., WEBER S., BALE R., WIDMANN G.: Comparison of freehand-navigated and aiming device-navigated targeting of liver lesions. *The International Journal of Medical Robotics and Computer Assisted Surgery* 10, 1 (2014), 35–43. 2